Numerical Analysis of Bifurcation Angles and Branch Patterns in Intracranial Aneurysm Formation

Tetsuo Sasaki, MD
Department of Neurosurgery, Shinshu University School of Medicine, Matsumoto, Japan

Yukinari Kakizawa, MD, PhD
Department of Neurosurgery, Shinshu University School of Medicine, Matsumoto, Japan

Masato Yoshino, PhD
Institute of Engineering, Academic Assembly, Shinshu University, Nagano, Japan
Institute of Carbon Science and Technology, Interdisciplinary Cluster for Cutting Edge Research, Shinshu University, Nagano, Japan

Yasuhiro Fujii, ME
Department of Mechanical Systems Engineering, Shinshu University, Nagano, Japan

Ikumi Yoroi, BE
Department of Mechanical Systems Engineering, Shinshu University, Nagano, Japan

Yozo Ichikawa, MD
Department of Neurosurgery, Shinshu University School of Medicine, Matsumoto, Japan

Tetsuyoshi Horiuchi, MD, PhD
Department of Neurosurgery, Shinshu University School of Medicine, Matsumoto, Japan

Kazuhiro Hongo, MD, PhD
Department of Neurosurgery, Shinshu University School of Medicine, Matsumoto, Japan

Correspondence to Tetsuo Sasaki, MD, Department of Neurosurgery, Shinshu University School of Medicine, 3-1-1 Asahi, Matsumoto 390-8621, Japan
Telephone: +81-263-37-2690
Fax: +81-263-37-0480
E-mail: sasakit@shinshu-u.ac.jp

Acknowledgments

None.

Disclosures

None.

The corresponding author was supported by Grants-in-Aid for Young Scientists (B); grant number 20791003 from the Ministry of Education, Culture, Sports, Science and Technology of Japan.

Abstract

Background: Hemodynamic factors, especially wall shear stress (WSS), are generally thought to play an important role in intracranial aneurysm (IA) formation. IAs frequently occur at bifurcation apices, where the vessels are exposed to the impact of WSS.

Objective: We aimed to elucidate the relationship between bifurcation geometry and WSS for IA formation.

Methods: Twenty-one bifurcation models varying in branch angles and branch diameters were made with 3-dimensional computer-aided design software. In all models, the value of maximum WSS (WSS_{MAX}), the area of high WSS (AREA), and the magnitude of wall shear force over AREA ($|\vec{F}_w|$) were investigated by the steady-flow simulation of computational fluid dynamics.

Results: On the basis of statistical analysis, WSS_{MAX} tended to be high when the bifurcation angle and/or branch diameter was small. AREA and $|\vec{F}_w|$ significantly increase as the bifurcation and/or the branch angle became larger.

Conclusions: The magnitude of WSS strongly correlated with bifurcation geometry. In addition to high WSS, AREA and $|\vec{F}_w|$ were thought to affect IA formation. Observed bifurcation geometry may predict IA formation. Large branch angles and small branch may increase the risk of IA formation.

Keywords: bifurcation, computational fluid dynamics, geometry, intracranial aneurysm, wall shear stress

Running title: Bifurcation geometry associated intracranial aneurysm formation

Abbreviations

3D CAD = 3-dimensional computer-aided design

AREA = the area of high WSS

CFD = computational fluid dynamics

$|\vec{F}_w|$ = the magnitude of wall shear force over AREA

IA = intracranial aneurysm

WSS = wall shear stress

WSS_{MAX} = the value of maximum WSS

WSSG = WSS gradient

Introduction

Hemodynamic factors play important roles in intracranial aneurysm (IA) formation.[1-6] IAs frequently occur at bifurcation apices, where the vessels are exposed to the impact of wall shear stress (WSS).[5-12] Recent studies show that high WSS regulates vessel endothelium function and causes inflammatory reactions in the vessel wall underlying aneurysm formation and growth.[5,6,9,13-16]

Some studies have shown that bifurcation angles or branch diameters affect IA development.[17-19] Alnæs et al.[18] used computational fluid dynamics (CFD) to investigate the impact of vessel radius and bifurcation angle variations on pressure and WSS in the complete circle of Willis. They found that deviations from normal anatomy resulted in redistribution of wall pressures and increased WSS. Although WSS magnitude likely depends on bifurcation geometry and may be a leading factor of IA formation, there are no detailed analyses of the relationship between bifurcation geometry and WSS. Therefore, we constructed basic bifurcation models with many variations and elucidated how bifurcation geometry influences IA formation by examining the WSS increase and distribution using CFD simulations.

Methods

Geometric Modeling

Many variations of three-dimensional computer-aided design (3D CAD) models were made using the 3D CAD engineering software (SolidWorks2009; Dessault Systèms SolidWorks Corp., Waltham, MA, USA) (Figure 1, Left). All models had a parent vessel (D_0) 4-mm in diameter to approximate major intracranial arteries, where IAs frequently occur. Bifurcation angles (ϕ_{L+R}) were set in five patterns at 60°, 90°, 120°, 150°, and 180°. Branch angles (ϕ_L or ϕ_R) were varied by 30° from 0° to 90°. Eight models (type A) had equal-diameter (3.175 mm) branches as the basic variations (Figure 1, Right-A). Additionally, 13 models (type B) had different-diameter branches (Figure 1, Right-B). The small-branch diameter (D_1) was 1.600 mm, and the large-branch diameter (D_2) was 3.913 mm. Branch diameters were determined according to Murray's law,[20] which is derived based on the basis of the mass conservation in the bifurcation. That is, $r_0^3 = r_1^3 + r_2^3$, where r_0 is the radius of the parent artery, and r_1 and r_2 are the radii of the branching arteries.

Numerical Simulation

The whole domain was divided into tetrahedral elements, and body-fitting meshes were used near the wall boundaries to perform accurate WSS calculation. The number of elements used in this study ranged from 900 000 to 1150 000. Blood was assumed as an incompressible Newtonian fluid with a density of 1060 kg/m^3 and viscosity of 4.24×10^{-3} Pa s. The vessel wall was considered rigid with a no-slip condition. A recent study showed that steady-state CFD solution virtually agrees (<3% WSS difference) with the average pulsatile CFD solution in animal models.[21] Indeed, although pulsatile-flow simulations should be done, our preliminary computations also indicated that the WSS magnitude trends were captured in steady-flow simulations. Therefore, steady-flow simulations were conducted for simplicity. At the inlet boundary, the uniform velocity was set to 0.425 m/s as the average peak systole and end diastole in the internal carotid artery.[22] At the outlet boundary, the flow-rate ratio of each branch was specified in proportion to the cross-sectional branch area ratio. The calculated Reynolds number was 425, defined by the uniform inflow velocity and the parent vessel's diameter; hence the flow was assumed laminar.[23] The continuity and Navier-Stokes equations for incompressible fluids with boundary conditions were solved by the commercial software ANSYS FLUENT 12.1 (ANSYS, Inc., Canonsburg, PA, USA). The numerical method was based on the SIMPLE algorithm[24] and the second-order upwind scheme for the convection terms. No turbulent models were used in computation. Steady-flow computations were repeated until a convergence criterion that the relative errors of the velocity components became < 10^{-5} for all grid points. In simulations, WSS magnitudes on each geometric model's boundary were calculated. Additionally, maximum value of WSS (WSS_{MAX}), area of high WSS (AREA), and magnitude of wall shear force over AREA ($|\vec{F}_w|$) were investigated. Note that AREA was defined as the area where WSS magnitude was ≥ 15 Pa, using a previously described threshold.[25] When AREA was continuous over both branches, it bisected the bifurcation angle to calculate the AREA of each branch (Figure 2, left). $\vec{F}_w$ magnitude was given as follows:

$$|\vec{F}_w| = \sum_{i=1}^{n} |\vec{\tau}_{wi}| A_i,$$

where $|\vec{\tau}_{wi}|$ is the magnitude of WSS vector on the boundary surface of the i-th element, and A_i is the area of the element ($i = 1, 2, \ldots, N$). Briefly, WSS (Pa) and WSS_{MAX} (Pa) are the forces per unit area, which are applied to one point on the vessel wall, AREA (mm^3) is the area of the vessel wall under high WSS(≥ 15 Pa), and $|\vec{F}_w|$ (10^{-6}N) is the sum of WSS over the AREA.

Statistical Analysis

WSS_{MAX}, AREA, and $|\vec{F}_w|$ were collected for all models. Each WSS parameter was compared against ϕ_{L+R} or either branch angle of interest (ϕ_L or ϕ_R) using univariate linear regression analysis. Dependent variables (WSS_{MAX}, AREA, and $|\vec{F}_w|$) were treated as continuous variables each to B_L and B_R, respectively. Independent variables (ϕ_{L+R}, ϕ_L and ϕ_R) were treated as continuous variables. Since dependent variables were treated as continuous variables, univariate linear regression analysis was used. The P values of the Wald test were described as the test of univariate analysis. $P < 0.05$ was considered statistically significant in each test using commercial software JMP 9 (SAS Institute Inc., Cary, NC, USA). Furthermore, multivariate linear regression analyses were added as independent variables of ϕ_L and ϕ_R. ϕ_{L+R} was not added as an independent variable in multivariate linear regression analyses because of the sum of ϕ_L and ϕ_R.

Results

Figure 2 (Right) shows WSS visualized with color-coded magnitudes in the 3-D geometric models. Peak WSS was found near the terminus of bifurcations in each model.

Table 1 shows bifurcation geometries and each WSS parameter for type A models. In the symmetrical models (A-1, A-5, A-8), WSS_{MAX} was highest in the model with the smallest ϕ_{L+R} (A-1), while AREA and $|\vec{F}_w|$ increased as ϕ_{L+R} increased. The site of WSS_{MAX} shifted distally from the apex as ϕ_{L+R} increased. In asymmetrical models with different branch angles (A-2, A-3, A-4, A-6, A-7), WSS_{MAX}, AREA and $|\vec{F}_w|$ were higher with large-branch than with small-branch angles. WSS_{MAX} was high when ϕ_{L+R} was small. There was a negative correlation between WSS_{MAX} of the interest branch and ϕ_{L+R} statistical significance with univariate linear regression analysis (Table 2). From multivariate linear regression analysis, association between WSS_{MAX} of the B_L and ϕ_{L+R} depended on ϕ_R, larger branch angle (Table 3). Association between WSS_{MAX} of the B_R and ϕ_{L+R} tended to depend on ϕ_R (Table 3). A positive correlation was shown between AREA of the interest branch and ϕ_{L+R} or the branch angle of the interest branch with univariate linear regression analysis (Table 2). From multivariate linear regression analysis, association between AREA of the B_L and ϕ_{L+R} depended on ϕ_L (Table 3). Association between AREA of the B_R and ϕ_{L+R} depended on both of ϕ_L and ϕ_R (Table 3). There was also a positive correlation between $|\vec{F}_w|$ of the interest branch and ϕ_{L+R} or the branch angle of the interest branch with univariate linear regression analysis (Table 2). From multivariate linear regression analysis, association between $|\vec{F}_w|$ of the B_L and ϕ_{L+R} depended on ϕ_L (Table 3). Association between $|\vec{F}_w|$ of the B_R and ϕ_{L+R} depended on both of ϕ_L and ϕ_R (Table 3). For type A, WSS_{MAX} was significantly higher when ϕ_{L+R} was small or branch angle was large. AREA and $|\vec{F}_w|$ were significantly higher when ϕ_{L+R} or the branch angle of the interest branch was larger.

For type B, irrespective of branch angles, WSS_{MAX} was high on small branches when ϕ_{L+R} was ≤ 120° (except for B-9) and on large branches when ϕ_{L+R} was ≥ 150°. AREA and $|\vec{F}_w|$ were greater for large branches in models having equal branch angles (B-1, B-8, B-13) and when ϕ_{L+R} was ≥ 150° (B-11, B-12); these indices were greater for large branch angles in other models (Table 4). There was a negative correlation between WSS_{MAX} of the small branch (B_L) and ϕ_{L+R} with univariate linear regression analysis (Table 5). From multivariate linear regression analysis, association between WSS_{MAX} of the B_L and ϕ_{L+R} depended on both of ϕ_L and ϕ_R (Table 6). Association between WSS_{MAX} of the B_R and ϕ_{L+R} depended on ϕ_L (Table 6). Irrespective of branch diameter, there was a positive correlation between AREA and ϕ_{L+R} with univariate linear regression analysis (Table 5). The relationship between AREA and ϕ_L was not observed, while there was a positive correlation between AREA and ϕ_R with univariate linear regression analysis (Table 5). From multivariate linear regression analysis, association between AREA of the B_L and ϕ_{L+R} depended on both of ϕ_L and ϕ_R (Table 6). Association between AREA of the B_R and ϕ_{L+R} depended on ϕ_R (Table 6). Similar tendency was shown in the relationship between $|\vec{F}_w|$ and ϕ_{L+R} or branch angles. For type B, WSS_{MAX} of the small branch was significantly higher when ϕ_{L+R} was small. AREA and $|\vec{F}_w|$ significantly correlated with ϕ_{L+R} and the angle of the large branch.

Our results suggest: 1) WSS_{MAX} tended to be high when bifurcation angle and/or branch diameter was small; and 2) AREA and $|\vec{F}_w|$ were significantly increased as bifurcation and/or branch angle increased.

Discussion

Common risk factors for IA formation such as hypertension, smoking, familial predisposition, and hemodynamic stress have been identified.[5] Hemodynamic factors are generally recognized to play an important role on IA formation.[1-6] IAs frequently occur in the circle of Willis, and in particular at apices of arterial bifurcations or at the branching points of a parent artery, where the vessels are exposed to the impact of WSS.[5-12] Hashimoto et al.[1] demonstrated that increased flow and systemic hypertension are required to create experimental IAs in rats. Observations from animal models showed that elevations of WSS caused alterations in endothelial phenotype, endothelial damage, and fragmentation of the internal elastic lamina.[2-4,8,10,11,26] Meng et al.[8] reported histopathological and hemodynamic analysis using IA models in dogs, in which aneurysmal initiation was observed at the site of high WSS and high WSS gradient (WSSG). Kulcsár et al.[27] analyzed CFD for 3 human-specific models in which IAs occurred, and demonstrated that both WSS and WSSG increased at the regions where IAs developed. Moreover, Alfano et al.[12] indicated that high WSS and high WSSG were found at bifurcations where IAs frequently occur. Accordingly, many studies support that high WSS is associated with the first stage in IA formation.[5-12,26,27]

The present study also showed that WSS_{MAX} tended to be high when a branch diameter was small as the previous reports.[18] However, the observation suggested that WSS_{MAX} was high when a bifurcation angle was small in the present study although the previous studies have shown that large branch angle was a risk factor of IA formation.[2,17,19] This paradoxical result may be explained by the following hypotheses: (1) actual cerebral arteries, particularly in the circle of Willis, hardly have sharp bifurcations;[17] (2) other hemodynamic parameters except for WSS_{MAX} may also affect IA formation. Mean arterial WSS in the straight segments of large arteries is recognized to be within the range of 1.5 to 2.0 Pa.[5,13,27] Although peak of WSS was observed near the terminus of bifurcations, the range of WSS_{MAX} by changes of bifurcation angles was not so large in the present study. In contrast, AREA and $|\vec{F}_w|$ were greater as bifurcation and/or branch angle became larger with strong correlation. Consequently, speculation would suggest that AREA and $|\vec{F}_w|$ affect IA formation as well as high WSS because a risk of IA formation seems to be higher by exposure of high WSS consistently and widely. AREA and $|\vec{F}_w|$ can be two of the factors to support the clinical observation that large bifurcation angle is a risk of IA formation. On the other hand, in type B models having different branches in diameter, WSS_{MAX} tended to be higher on small branch by a correlation analysis, whereas there was no correlation between a branch diameter and AREA or $|\vec{F}_w|$. These observations might be brought by the difference of the area of high velocity gradient near the vessel wall between different branches in diameter. That is, in a part of type B models, AREA of large branch would be greater than one of small branch because the area of high velocity gradient near the vessel wall in large branch was greater than that in small branch. We thought that further studies to investigate the relationships between WSS and a branch diameter would be needed using additional models having variations of branch diameters. The present study suggested that small branch would be a risk factor of IA formation because statistical significance was shown between elevation of WSS_{MAX} and small branch. Actually, aneurysmal necks often ride the side of small branch at bifurcation, such as the middle cerebral artery and the posterior communicating artery (Figures 3 and 4). Therefore, care should be taken of bifurcation geometry to avoid recurrence in aneurysmal clipping, such as obliteration of aneurysmal neck especially of the side of small branch and addition of wrapping distally to bifurcation apices. Tight packing for the area of high WSS which occurs to aneurysmal orifice after aneurysmal obliteration is recommended in endovascular coiling for cerebral aneurysms.

Recently, although other hemodynamic parameters contributing to IA formation have been proposed including WSSG,[8,9,12,27] oscillatory shear index (OSI),[25,28] aneurysm formation indicator (AFI)[29] and gradient oscillatory number (GON),[30] these indices are short of evidences compared with WSS. However, WSSG has been considered to be one of leading factors in IA formation, and the research on relationship between WSSG and bifurcation geometry should be our future subject.

Although a number of CFD studies were analyzed using the realistic vessel models created by angiography of patients or healthy volunteers, we considered the following problems of CFD simulations to investigate the relationship between bifurcation geometry and WSS using the patient-specific models: (1) it is complicated to produce the models varied bifurcation angle or branch diameter; (2) measurement errors between imaging modalities in modeling can occur.[31] In contrast, exact adjustment of angles and diameters is possible in simple models as the present study, and production of many models is also easy. Moreover, with simple models used, comparison of hemodynamic indices between each model should be advantageous, and numerical reproducibility can be high.

Recent studies have disclosed that high WSS regulates the functions of the vessel endothelium and it causes inflammatory reactions in the vessel wall underlying aneurysm formation and growth.[5,6,9,13-16] Furthermore, the medicine with an anti-inflammatory effect is thought to have a possibility of cure for IAs. Aoki et al.[32,33] demonstrated that statins could inhibit the progression of IAs in animal models. The present study suggests that high and regional WSS was shown when a bifurcation angle was small and when a branch diameter was small. In contrast, the area exposed to high WSS was greater as a branch angle became larger. By getting to know characteristic vessel geometries which have a potential risk of IA formation, intervention of preventive medication as well as close follow-up may be recommended for such cases. Furthermore, in cases where the vessels have risky bifurcation geometries, careful follow-up should be done and it may be considered to perform wrapping if there is an opportunity of direct observation in craniotomy. Although the simulations using the patient-specific models seem to be a better way when investigating a risk of IA formation, it generally requires complicated processes to calculate the hemodynamic parameters. Actually, we think that it is simple and practical to make bifurcation geometry into an indicator of IA formation.

Limitations of the Study

There are several limitations in the present study. The first limitation is the difference of bifurcation geometry between simple models and human vessels. We herein designed the bifurcation geometry only including branches in a two-dimensional plane because of very complicated analyses in a three-dimensional model. Actual bifurcations of the cerebral arteries have complex structures such as tortuous vessels, irregular vessel diameters, and others. Additionally, to include the vessel elasticity into CFD simulations is technically difficult. Furthermore, boundary conditions are changed by a range of vessel length or flow rate,[34,35] so it is difficult to measure the values of hemodynamic parameters correctly. Therefore, the results of the present study can not necessarily suit human vessels. In future work, further investigations by using more complicated geometry models and many patient-specific models are required to verify the relationship between these models and clinical IA formation. The second limitation is that similar hemodynamic change is not necessarily observed in side-wall aneurysms occurring at the non-branching site. In side-wall aneurysms, it is unclear whether WSS in the site of IA formation is high or low.[27,30] IA formation has a multifactorial etiology, so other factors may affect side-wall aneurysms although WSS is a strong candidate of IA formation.[7] Hemodynamic analysis of non-branching vessels remains as a future subject. Many limitations still remain in CFD studies, whereas by the development of computer technology and biorheology, it is expected that those problems will be solved in the near future.

Conclusions

The magnitude of WSS strongly correlated with bifurcation geometry. The present study suggested that high and regional WSS was shown when a bifurcation angle was smaller and when a branch diameter was small. In contrast, the area exposed to high WSS was greater as bifurcation and/or branch angle became larger. In addition to high WSS, the area of high WSS and the magnitude of wall shear force over the area were thought to affect IA formation. Observed bifurcation geometry would be a predictor for IA formation. Large branch angles and small branches can be a potential risk factor of IA formation.

References

1. Hashimoto N, Handa H, Hazama F. Experimentally induced cerebral aneurysms in rats. *Surg Neurol*. 1978;10:3-8.
2. Stehbens WE. Etiology of intracranial berry aneurysms. *J Neurosurg.* 1989;70:823-831.
3. Morimoto M, Miyamoto S, Mizoguchi A, Kume N, Kita T, Hashimoto N. Mouse model of cerebral aneurysm: experimental induction by renal hypertension and local hemodynamic changes. *Stroke*. 2002;33:1911-1915.
4. Gao L, Hoi Y, Swartz DD, Kolega J, Siddiqui A, Meng H. Nascent aneurysm formation at the basilar terminus induced by hemodynamics. *Stroke*. 2008;39:2085-2090.
5. Nixon AM, Gunel M, Sumpio BE. The critical role of hemodynamics in the development of cerebral vascular disease. *J Neurosurg*. 2010;112:1240-1253.
6. Meng H, Tutino VM, Xiang J, Siddiqui A. High WSS low WSS? Complex interactions of hemodynamics with intracranial aneurysm initiation, growth, and rupture: toward a unifying hypothesis. *AJNR Am J Neuroradiol.* 2014;35:1254-1262.
7. Foutrakis GN, Yonas H, Sclabassi RJ. Saccular aneurysm formation in curved and bifurcating arteries. *AJNR Am J Neuroradiol*. 1999;20:1309-1317.
8. Meng H, Wang Z, Hoi Y, et al. Complex hemodynamics at the apex of an arterial bifurcation induces vascular remodeling resembling cerebral aneurysm initiation. *Stroke*. 2007;38:1924-1931.
9. Wang Z, Kolega J, Hoi Y, et al. Molecular alterations associated with aneurysmal remodeling are localized in the high hemodynamic stress region of created carotid bifurcation. *Neurosurgery*. 2009;65:169-177.
10. Metaxa E, Tremmel M, Natarajan SK, Xiang J, Paluch RA, Mandelbaum M, et al. Characterization of critical hemodynamic contributing to aneurysmal remodeling at the basilar terminus in a rabbit model. *Stroke*. 2010;41:1774-1782

11. Meng H, Metaxa E, Gao L, et al. Progressive aneurysm development following hemodynamic insult. *J Neurosurg*. 2011;114:1095-1103.

12. Alfano JM, Kolega J, Natarajan SK, et al. Intracranial aneurysms occur more frequently at bifurcation sites that typically experience higher hemodynamic stresses. *Neurosurgery*. 2013;73:497-505.

13. Hashimoto, T, Meng H, Young WL. Intracranial aneurysms: links among inflammation, hemodynamics and vascular remodeling. *Neurol Res*. 2006;28:372-380.

14. Aoki T, Nishimura M. The development and the use of experimental animal models to study the underlying mechanisms of CA formation. *J Biomed Biotechnol*. 2011;doi:10.1155/2011/535921.

15. Kolega J, Gao L, Mandelbaum M, et al. Cellular and morecular responses of the basilar terminus to hemodynamics during intracranial aneurysm initiation in a rabbit model. *J Vasc Res*. 2011;48:429-442.

16. Chalouhi N, Ali MS, Jabbour PM, et al. Biology of intracranial aneurysms: role of inflammation. *J Cereb Blood Flow Metab*. 2012;32:1659-1676.

17. Ingebrigtsen T, Morgan MK, Faulder K, Ingebrigtsen L, Sparr T, Schirmer H. Bifurcation geometry and the presence of cerebral artery aneurysms. *J Neurosurg*. 2004;101:108-113.

18. Alnæs MS, Isaksen J, Mardal KA, Romner B, Morgan MK, Ingebrigsten T. Computation of hemodynamics in the circle of Willis. *Stroke*. 2007;38:2500-2505.

19. Bor AS, Velthuis BK, Majoie CB, Rinkel GJ. Configuration of intracranial arteries and development of aneurysms: a follow-up study. *Neurology*. 2008;70:700-705.

20. Murray CD. The physiological principle of minimum work applied to the angle of branching of arteries. *J Gen Physiol*. 1926;9:835-841.

21. Tremmel M, Xiang J, Hoi Y, et al. Mapping vascular response to in vivo hemodyanamics: application to increased flow at the basilar terminus. *Biomech Model Mechanobiol.*

2010;9:421-434.

22. Shojima M, Oshima M, Takagi K, et al. Role of the bloodstream impacting force and the local pressure elevation in the rupture of cerebral aneurysms. *Stroke*. 2005;36:1933-1938.

23. Gijsen FJ, van de Vosse FN, Janssen JD. The influence of the non-Newtonian properties of blood flow in large arteries: steady flow in a carotid bifurcation model. *J Biomech*. 1999;32:601-608.

24. Patankar S.V. Numerical Heat Transfer and Fluid Flow, McGraw-Hill, New York. 1980.

25. Singh PK, Marzo A, Howard B, et al. Effects of smoking and hypertension on wall shear stress and oscillatory shear index at the site of intracranial aneurysm formation. *Clin Neurol Neurosurg*. 2010;112:306-313.

26. Steiger HJ. Pathophysiology of development and rupture of cerebral aneurysms. *Acta Neurochir Suppl (Wien)*. 1990;48:1-57.

27. Kulcsár Z, Ugron A, Marosfoi M, Berentei Z, Paál G, Szikora I. Hemodynamics of cerebral aneurysm initiation: the role of wall shear stress and spatial wall stress gradient. *AJNR Am J Neuroradiol*. 2011;32:587-594.

28. He X, Ku DN. Pulsatile flow in the human left coronary artery bifurcation: average conditions. *J Biomech Eng* 1996;118:74-82

29. Mantha A, Karmonik C, Benndorf G, Strother C, Metcalfe R. Hemodynamics in a cerebral artery before and after the formation of an aneurysm. *AJNR Am J Neuroradiol*. 2006;27:1113-1118.

30. Shimogonya Y, Ishikawa T, Imai Y, Matsuki N, Yamaguchi T. Can temporal fluctuation in spatial wall stress gradient initiate a cerebral aneurysm? A proposed novel hemodynamic index, the gradient oscillatory number (GON). *J Biomech*. 2009;42:550-554.

31. Geers AJ, Larrabide I, Radaelli AG, et al. Patient-specific computational hemodynamics of intracranial aneurysms from 3D rotational angiography and CT angiography: an in

vivo reproducibility study. *AJNR Am J Neuroraidol*. 2011;32:581-586.

32. Aoki T, Kataoka H, Ishibashi R, Nozaki K, Hashimoto N. Simvastatin suppresses the progression of experimentally induced cerebral aneurysms in rats. *Stroke*. 2008;39:1276-1285.
33. Aoki T, Kataoka H, Ishibashi R, et al. Pitavastatin suppresses formation and progression of cerebral aneurysms through inhibition of the nuclear factor kappaB pathway. *Neurosurgery*. 2009;64:357-365.
34. Castro MA, Putman CM, Cebral JR. Coumputational fluid dynamics modeling of intracranial aneurysms: effects of parent artery segmentation on intra-aneurysmal hemodynamics. *AJNR Am J Neuroradiol*. 2006;27:1703-1709.
35. Venugopal P, Valentiono D, Schmitt H, Villablanca JP, Viñuela F, Duckwiler G. Sensitivity of patient-specific numerical simulation of cerebral aneurysm hemodynamics to inflow boundary conditions. *J Neurosurg*. 2007;106:1051-1060.

Figure legends

Figure 1. Left: An example of the bifurcation model with three-dimensional computer aided design (3-D CAD). The diameter of the parent vessel (D_0) is fixed at 4 mm, and the parent vessel divided into small branch (D_1) and large branch (D_2). Branch angles are represented as ϕ_L and ϕ_R, respectively. The bifurcation angle (ϕ_{L+R}) is denoted by the sum of ϕ_L and ϕ_R. **Right:** All 21 models with variations of the bifurcation geometry. Bifurcation angles (ϕ_{L+R}) are set in five patterns at 60°, 90°, 120°, 150°, and 180°. Branch angles (ϕ_L or ϕ_R) are varied by 30° from 0° to 90°. The 8 models have equal branches in diameter as the basic variations (A). Both branch diameters are 3.175 mm. The 13 models have different branches in diameter (B). The diameter of small branch (D_1) is 1.600 mm, and that of large branch (D_2) is 3.913 mm. Each branch diameter is decided by Murray's law.

Figure 2. Left: An example of the area of high WSS with ≥ 15 Pa (AREA). When AREA is continuous over both branches as this sample, it is divided in bisector of a bifurcation angle to calculate AREA of each branch. **Right:** The distribution of wall shear stress (WSS) visualized with color-coded magnitudes in the 3-D geometric models. The basic models having equal diameter branches (A), and another models having different diameter branches (B). Peak WSS is found near the terminus of bifurcations in each model. Maximum value of WSS (WSS_{MAX}) is shown as each arrow except for symmetrical models (A-1, A-5, A-8).

Figure 3. Computational tomography angiogram in the patient of 71-year-old man showing the right middle cerebral artery unruptured aneurysm. The aneurysmal neck distributes from the bifurcation apex to the small branch having larger branch angle.

Figure 4. A patient-based model from computational tomography angiogram in the case (58-year-old woman) of the left internal carotid artey unruptured aneurysm (A), an aneurysm removal model (B) and a steady-flow simulation model for WSS (C). Numerical analysis was conducted under the same conditions as the present study. High WSS was observed from the apex of the bifurcation to the posterior communicating artery (arrow).

Figure 1

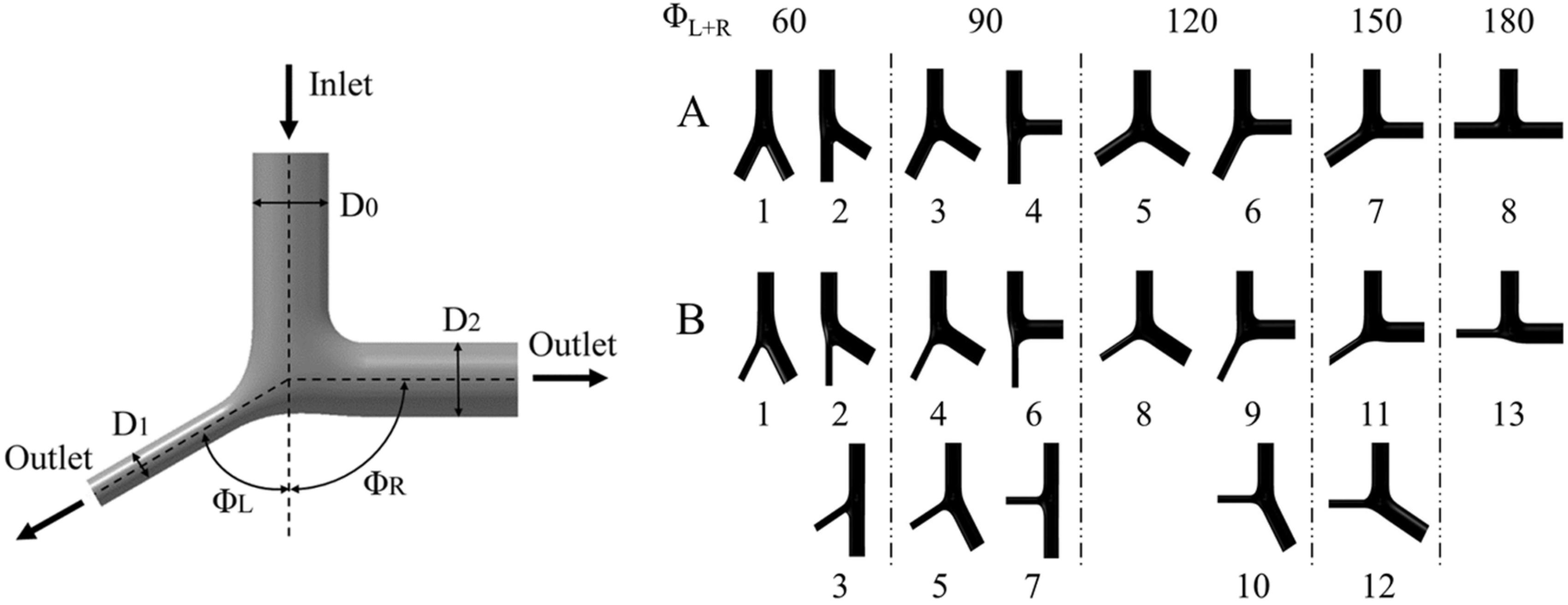

Inlet
D0
D2
Outlet
D1
Outlet
ΦL
ΦR
ΦL+R
60
90
120
150
180
A
1
2
3
4
5
6
7
8
B
1
2
4
6
8
9
11
13
3
5
7
10
12

Figure 2

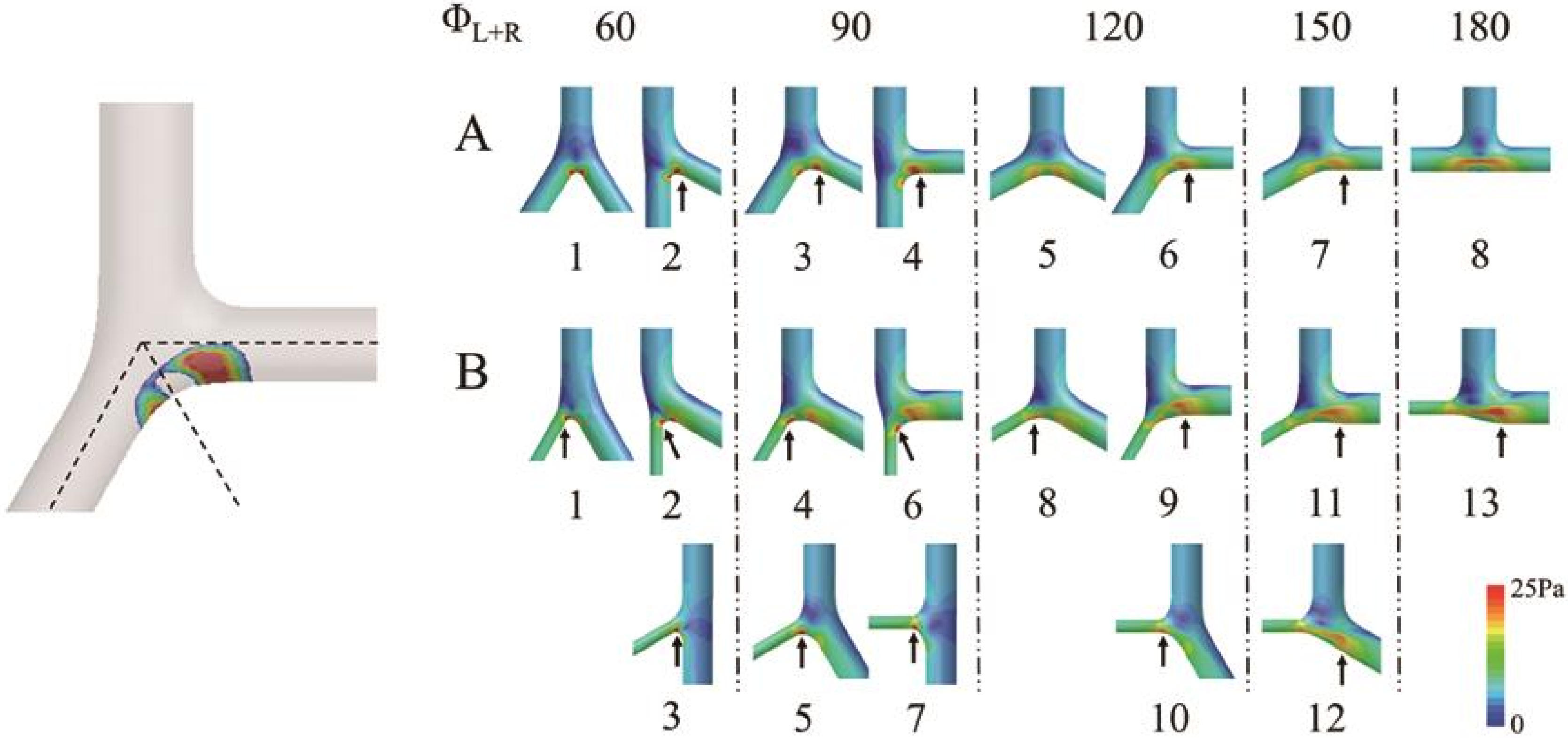

Φ_{L+R}
60
90
120
150
180
A
1
2
3
4
5
6
7
8
B
1
2
4
6
8
9
11
13
3
5
7
10
12
25Pa
0

Figure 3

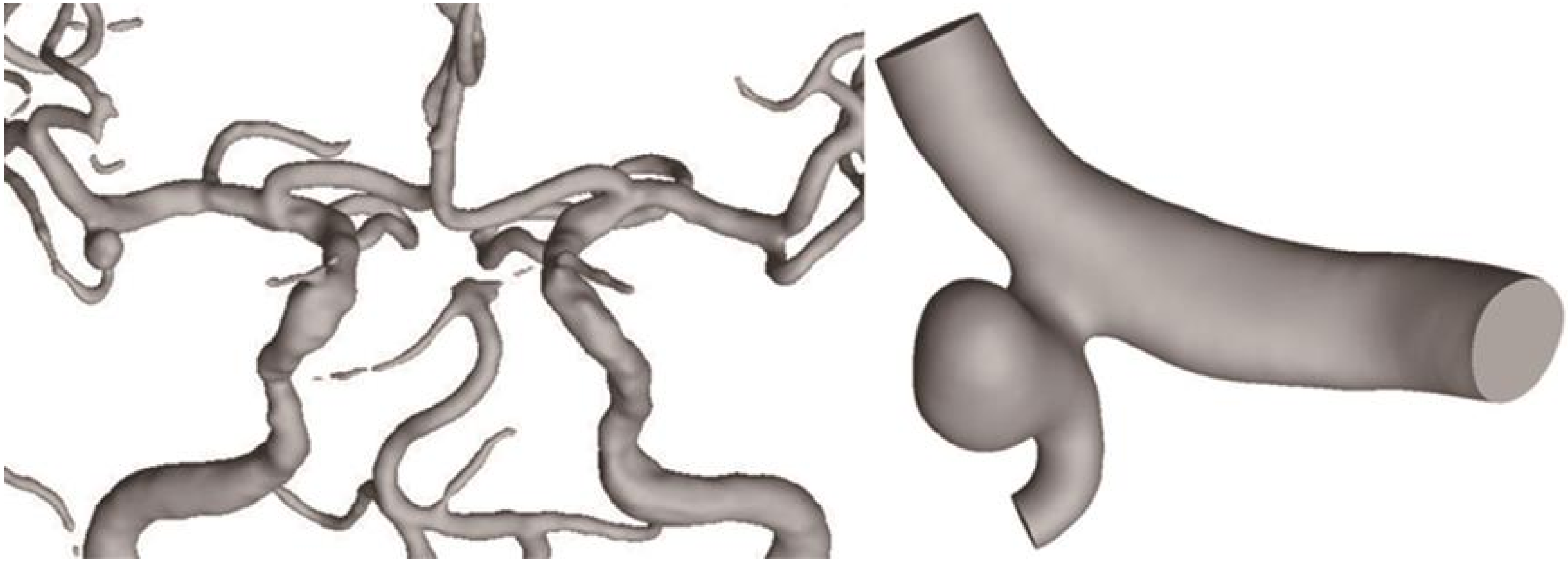

Figure 4

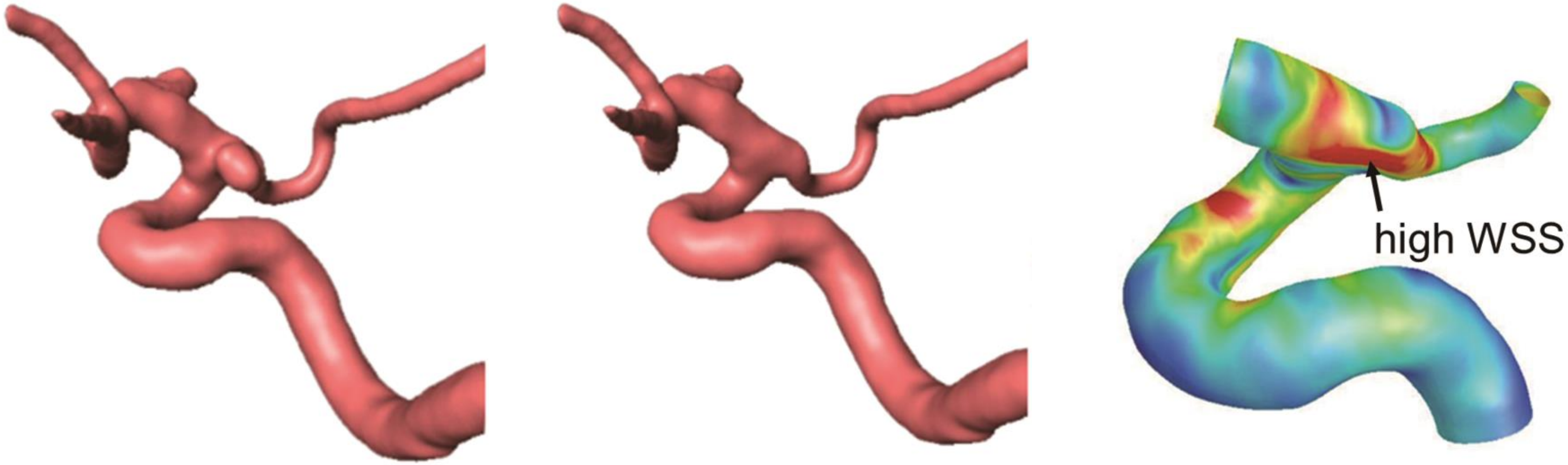

A B C

Table 1. The data of bifurcation geometries and hemodynamic parameters in type A models

	ϕ_{L+R} (°)	ϕ_L (°)	ϕ_R (°)	WSS_{MAX} (Pa)		AREA (mm^2)		$\lvert \vec{F}_w \rvert$ (10^{-6}N)	
				B_L	B_R	B_L	B_R	B_L	B_R
A-1	60	30	30	42.1	43.9	3.52	3.53	85.8	85.7
A-2	60	0	60	36.5	43.1	2.32	4.78	55.1	114
A-3	90	30	60	26.5	27.6	5.76	7.54	114	151
A-4	90	0	90	23.8	27.4	3.74	10.6	70.8	215
A-5	120	60	60	21.5	21.5	10.2	10.2	183	183
A-6	120	30	90	20.8	22.5	6.30	13.5	109	254
A-7	150	60	90	18.0	20.9	9.17	15.0	150	264
A-8	180	90	90	24.3	24.3	15.6	15.6	285	285

ϕ_{L+R}: bifurcation angle, ϕ_L: angle of the left branch, ϕ_R: angle of the right branch, B_L: the left branch, B_R: the right branch, WSS: wall shear stress, WSS_{MAX}: the value of maximum WSS, AREA: the area of high WSS (≥ 15 Pa), $\lvert \vec{F}_w \rvert$: wall shear force of over the area of high WSS (≥ 15 Pa)

Table 2. Statistical analysis for testing correlation between bifurcation geometries and hemodynamic parameters in type A models

Regression analysis by univariate linear regression model

		ϕ_{L+R}		ϕ_L		ϕ_R	
		coefficient (95%CI)	p-value	coefficient (95%CI)	p-value	coefficient (95%CI)	p-value
WSS_{MAX}	B_L	-0.146 (-0.252,30.344)	3.518E-02†	-0.114 (-0.308,21.737)	2.951E-01	-0.303 (-0.477,35.415)	1.404E-02†
	B_R	-0.175 (-0.283,35.369)	1.956E-02†	-0.166 (-0.367,25.582)	1.571E-01	-0.305 (-0.535,33.638)	4.007E-02†
AREA	B_L	0.097 (0.067,-6.978)	7.443E-04†	0.135 (0.100,0.373)	2.637E-04†	0.087 (-0.055,-9.613)	2.765E-01
	B_R	0.100 (0.069,-4.384)	7.129E-04†	0.093 (0.002,2.332)	9.159E-02	0.180 (0.104,-8.355)	3.572E-03†
$\lvert \vec{F}_w \rvert$	B_L	1.557 (0.889,-115.032)	3.812E-03†	2.284 (1.687,17.593)	2.920E-04†	1.155 (-1.356,-137.079)	4.020E-01
	B_R	1.563 (0.971,-44.429)	2.059E-03†	1.334 (-0.216,70.447)	1.426E-01	3.014 (1.997,-96.313)	1.142E-03†

ϕ_{L+R}: bifurcation angle, ϕ_L: angle of the left branch, ϕ_R: angle of the right branch, B_L: the left branch, B_R: the right branch, WSS: wall shear stress, WSS_{MAX}: the value of maximum WSS, AREA: the area of high WSS (≥ 15 Pa), $\lvert \vec{F}_w \rvert$: wall shear force of over the area of high WSS (≥ 15 Pa)

[†]Statistically significant

Table 3. Statistical analysis for testing correlation between bifurcation geometries and hemodynamic parameters in type A models

Regression analysis by multivariate linear regression model

Dependent variables		Independent variables			
		ϕ_L		ϕ_R	
		coefficient (95%CI)	p-value	coefficient (95%CI)	p-value
WSS_{MAX}	B_L	-0.067 (-0.194,-0.282)	3.531E-01	-0.282 (-0.460,-0.282)	2.661E-02†
	B_R	-0.121 (-0.273,-0.266)	1.783E-01	-0.266 (-0.478,-0.266)	5.672E-02
AREA	B_L	0.127 (0.101,0.045)	2.270E-04†	0.045 (0.009,0.045)	6.020E-02
	B_R	0.066 (0.046,0.158)	1.463E-03†	0.158 (0.130,0.158)	1.148E-04†
$\lvert \vec{F}_w \rvert$	B_L	2.211 (1.598,0.442)	8.742E-04†	0.442 (-0.411,0.442)	3.563E-01
	B_R	0.879 (0.588,2.731)	1.964E-03†	2.731 (2.326,2.731)	4.422E-05†

ϕ_L: angle of the left branch, ϕ_R: angle of the right branch, B_L: the left branch, B_R: the right branch, WSS: wall shear stress, WSS_{MAX}: the value of maximum WSS, AREA: the area of high WSS (≥ 15 Pa), $\lvert \vec{F}_w \rvert$: wall shear force of over the area of high WSS (≥ 15 Pa)

†Statistically significant

Table 4. The data of bifurcation geometries and hemodynamic parameters in type B models

	ϕ_{L+R} (°)	ϕ_L (°)	ϕ_R (°)	Branch diameter (mm)		WSS_{MAX} (Pa)		AREA (mm^2)		$\lvert\vec{F}_w\rvert$ (10^{-6}N)	
				B_L (D_1)	B_R (D_2)	B_L	B_R	B_L	B_R	B_L	B_R
B-1	60	30	30	1.600	3.913	55.1	27.0	2.21	2.96	58.3	59.5
B-2	60	0	60	1.600	3.913	58.2	32.7	2.11	5.61	55.8	113
B-3	60	60	0	1.600	3.913	55.7	21.7	2.15	1.08	54.5	19.6
B-4	90	30	60	1.600	3.913	32.1	24.5	4.63	10.3	97.3	190
B-5	90	60	30	1.600	3.913	29.2	18.7	4.05	3.46	82.6	57.5
B-6	90	0	90	1.600	3.913	29.2	24.1	3.91	21.3	79.3	392
B-7	90	90	0	1.600	3.913	29.3	13.5	3.52	0	70.5	0
B-8	120	60	60	1.600	3.913	22.7	17.5	5.56	8.75	100	142
B-9	120	30	90	1.600	3.913	21.9	23.7	6.53	23.9	115	436
B-10	120	90	30	1.600	3.913	22.1	15.1	5.31	0.023	97	0.348
B-11	150	60	90	1.600	3.913	20.0	24.2	7.99	25.6	132	459
B-12	150	90	60	1.600	3.913	20.1	22.3	10.0	15.7	172	274
B-13	180	90	90	1.600	3.913	21.5	26.8	11.7	25.5	199	473

ϕ_{L+R}: bifurcation angle, ϕ_L: angle of the left branch, ϕ_R: angle of the right branch, B_L: the left branch, B_R: the right branch, D_1: small branch diameter, D_2: large branch diameter, WSS: wall shear stress, WSS_{MAX}: the value of maximum WSS, AREA: the area of high WSS (≥ 15 Pa), $\lvert\vec{F}_w\rvert$: wall shear force of over the area of high WSS (≥ 15 Pa)

Table 5. Statistical analysis for testing correlation between bifurcation geometries and hemodynamic parameters in type B models

Regression analysis by univariate linear regression model

		ϕ_{L+R}		ϕ_L		ϕ_R	
		coefficient (95%CI)	p-value	coefficient (95%CI)	p-value	coefficient (95%CI)	p-value
WSS_{MAX}	B_L (D_1)	-0.316 (-0.440,51.699)	4.055E-04†	-0.221 (-0.445,29.925)	8.064E-02	-0.204 (-0.434,28.715)	1.101E-01
	B_R (D_2)	-0.015 (-0.096,14.973)	7.185E-01	-0.102 (-0.175,23.362)	1.912E-02†	0.081 (0.000,13.104)	7.576E-02
AREA	B_L (D_1)	0.077 (0.066,-4.024)	2.049E-08†	0.049 (0.004,-0.085)	5.800E-02	0.054 (0.011,-0.223)	3.338E-02†
	B_R (D_2)	0.181 (0.067,-20.952)	9.949E-03†	-0.038 (-0.218,2.021)	6.839E-01	0.282 (0.210,-8.310)	9.694E-06†
$\lvert \vec{F}_w \rvert$	B_L (D_1)	1.111 (0.900,-40.718)	5.526E-07†	0.701 (0.016,21.590)	7.004E-02	0.793 (0.145,18.915)	3.536E-02†
	B_R (D_2)	3.229 (1.109,-379.451)	1.240E-02†	-0.803 (-4.075,41.901)	6.402E-01	5.142 (3.839,-152.123)	9.010E-06†

ϕ_{L+R}: bifurcation angle, ϕ_L: angle of the left branch, ϕ_R: angle of the right branch, B_L: the left branch, B_R: the right branch, D_1: small branch diameter, D_2: large branch diameter, WSS: wall shear stress, WSS_{MAX}: the value of maximum WSS, AREA: the area of high

WSS (≥ 15 Pa), $|\vec{F}_w|$: wall shear force of over the area of high WSS (≥ 15 Pa)
†Statistically significant

Table 6. Statistical analysis for testing correlation between bifurcation geometries and hemodynamic parameters in type B models

Regression analysis by multivariate linear regression model

Dependent variables		Independent variables			
		ϕ_L		ϕ_R	
		coefficient (95%CI)	p-value	coefficient (95%CI)	p-value
WSS_{MAX}	B_L	-0.322 (-0.481,-0.310)	2.682E-03†	-0.310 (-0.469,-0.310)	3.442E-03†
	B_R	-0.084 (-0.158,0.054)	4.878E-02†	0.054 (-0.020,0.054)	1.834E-01
AREA	B_L	0.075 (0.062,0.079)	7.361E-07†	0.079 (0.065,0.079)	4.717E-07†
	B_R	0.061 (-0.010,0.302)	1.236E-01	0.302 (0.231,0.302)	7.836E-06†
$\lvert\vec{F}_w\rvert$	B_L	1.077 (0.807,1.146)	1.435E-05†	1.146 (0.876,1.146)	8.276E-06†
	B_R	0.990 (-0.320,5.467)	1.693E-01	5.467 (4.157,5.467)	9.713E-06†

ϕ_L: angle of the left branch, ϕ_R: angle of the right branch, B_L: the left branch, B_R: the right branch, WSS: wall shear stress, WSS_{MAX}: the value of maximum WSS, AREA: the area of high WSS (≥ 15 Pa), $\lvert\vec{F}_w\rvert$: wall shear force of over the area of high WSS (≥ 15 Pa)

†Statistically significant